

Robust Packing Patterns and Luminescence Quenching in Mononuclear $[\text{Cu(II)}(\text{phen})_2]$ Sulfates

Elena Melnic,[†] Eduard B. Coropceanu,[‡] Olga V. Kulikova,[†] Anatolii V. Siminel,[†] Dane Anderson,[§] Hector J. Rivera-Jacquez,[§] Artëm E. Masunov,^{*,§,||} Marina S. Fonari,^{*,†} and Victor Ch. Kravtsov[†]

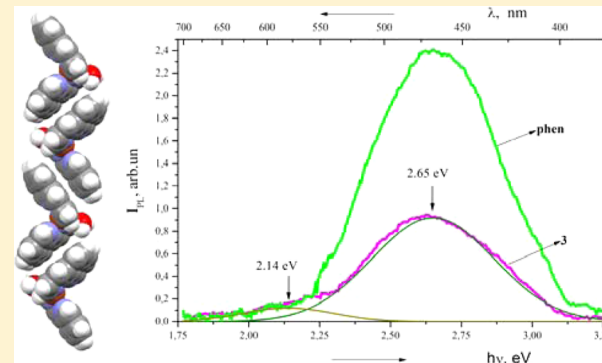
[†]Institute of Applied Physics and [‡]Institute of Chemistry, Academy of Sciences of Moldova, Academy Strasse 5, MD2028 Chisinau, Republic of Moldova

[§]NanoScience Technology Center, and Department of Chemistry, Department of Physics, and Florida Solar Energy Center, University of Central Florida, Orlando, Florida 32826, United States

^{||}Photochemistry Center RAS, ul. Novatorov 7a, Moscow, 119421, Russia

S Supporting Information

ABSTRACT: Three mixed-ligand Cu(II) complexes with compositions $[\text{Cu}(\text{phen})_2(\text{SO}_4)] \cdot \text{CH}_3\text{OH}$ (**1**), $[\text{Cu}(\text{phen})_2(\text{SO}_4)] \cdot (\text{H}_2\text{O})_2(\text{dmf})$ (**2**), and $[\text{Cu}(\text{phen})_2\text{H}_2\text{O}] (\text{SO}_4)(\text{H}_2\text{O})_4$ (**3**), where phen = 1,10-phenanthroline and dmf = N,N'-dimethylformamide, were prepared and studied. These compounds belong to the landscape of the mononuclear $\text{Cu}(\text{phen})_2$ sulfates, and the solvated complexes undergo frequent anion/water exchange at the metal center in aqueous solutions. Complexes are similar by the metal trigonal bipyramidal coordination geometry but differ by the mode of enclathration and number of protic and aprotic solvent guest molecules being accommodated in the crystal lattice. Crystal packing in **1–3** is determined by the robust supramolecular patterns that consist of stacking interactions between the planar extended phen fragments. These are observed in all three solids regardless of the interplay of other noncovalent interactions, including rather strong hydrogen bonds. The dual luminescence is detected at 580 and 470 nm for both crystals of phen and **3**. Detailed analysis of singlet and triplet excitations in phen and **3** is performed by time-dependent density functional methods. Fluorescence is predicted with a low quantum yield at 386 nm, and dual phosphorescence from $n-\pi^*$ and $\pi-\pi^*$ triplet states is predicted at 523 and 496 nm. Emission quenching was demonstrated for **3** and explained by nonradiative decay involving supramolecular stacking and low-lying metal-centered states.



INTRODUCTION

For decades Cu(II) coordination compounds have been attractive targets for magneto- and biochemistry.^{1,2} Engineering of metal–organic materials with specific properties using a molecular building blocks approach is possible only by understanding the interplay of different interactions involved in self-assembly processes. From a crystal engineering perspective, one of the advantages of using transition metal ions is that the shape of the main building block can be controlled by way of organic ligand-bound metal-containing modules in directions dictated by the coordination geometry of the metal center and by careful choice of the ligands.^{3–8} Design strategies employing simultaneously coordination bonds, hydrogen bonds, and $\pi-\pi$ stacking interactions in crystal engineering are mostly not well documented so far.⁹ We are involved in engineering, structural studies, and evaluation of properties of low-dimensional clusters and coordination polymers that include the Cu(II)–phen building block and reveal the contribution of stacking interactions in the crystal packing.^{10,11} The necessity of careful examination and

disclosure of the robust recurring patterns in such low-dimensional solids is dictated by their wide exploitation as medicinal forms with obvious antitumor efficacy. It has been reported that, in particular, phen derivatives $[\text{Cu}(\text{CH}_3\text{COO})_2(\text{phen})]$ and $[\text{Cu}(\text{sal})(\text{phen})]$ demonstrate approximately seven times higher activity than cisplatin against HepG2, A-498, and A-549 cancer cells. Among the factors that influence the cytotoxic activity, the planarity of N,N-diimine aromatic ligands plays a determinant role, as demonstrated by the higher efficacy of phen derivatives compared to bipyridine ones.² A number of complexes adopting a twisted $[\text{Cu}(\text{phen})_2]$ configuration defined by the two phen ligands being virtually orthogonal were proposed as metal-based synthetic nucleases able to bind and cleave DNA with or without addition of redox cofactors.¹² On the other hand, indications for the correlation between Alzheimer's

Received: August 25, 2014

Revised: November 8, 2014

Published: December 11, 2014

disease and Cu(II) uptake are increasing, and Cu(II) chelators are considered as a possible therapy for Alzheimer's disease. Observation of the highly specificity for Cu(II) in comparison with the other transition metals quenching effect for Alzheimer's amyloid- β peptide ($A\beta$) fluorescence makes a significant contribution to understanding the mode of Cu(II) binding to $A\beta$ in solution.^{13–15} From this viewpoint the mode of substrate–receptor interactions and impact of different intermolecular forces to the overall system of interactions are among the key factors to rationalize.

Taking into account growing interest in low-dimensional Cu(II) coordination compounds, we report herein the structures of three new Cu-(*phen*)₂ sulfates, [Cu(*phen*)₂(SO₄)] \cdot CH₃OH (1), [Cu(*phen*)₂(SO₄)](H₂O)₂(dmf) (2), and [Cu(*phen*)₂H₂O](SO₄)(H₂O)₄ (3), where *phen* = 1,10-phenanthroline and dmf = *N,N'*-dimethylformamide. The listed compounds extend the existing landscape of the [Cu(*phen*)₂SO₄] solvates and allow analyzing the interplay of intermolecular forces and modes of enclathration of protic and aprotic solvent guest molecules in the crystal lattice of the [Cu(*phen*)₂SO₄] scaffold. The TD-DFT calculations reveal the mechanism of dual luminescence by compound 3 as phosphorescence from $n-\pi^*$ and $\pi-\pi^*$ triplet states and explain its quenching by supramolecular π stacking in a H-aggregate pattern.

EXPERIMENTAL AND COMPUTATIONAL DETAILS

Materials and Physical Measurements. All reagents and solvents were obtained from commercial sources and used without further purification. Elemental analyses were performed on an Elementar Analysensysteme GmbH Vario El III 71 elemental analyzer. IR spectra were obtained as Nujol mulls on a FT IR Spectrum-100 PerkinElmer spectrometer in the range of 400–4000 cm^{−1}. Emission spectra were measured for the solids at room temperature on an Excitation YAG:Nd³⁺ laser, third-harmonic generation, k = 355 nm, duration = 10 ns, time repetition 10 Hz. Full synthetic details are provided in the Supporting Information.

X-ray Diffraction Studies. X-ray data for 1–3 were collected at room temperature on an Oxford Diffraction Xcalibur diffractometer equipped with a CCD area detector and a graphite monochromator utilizing Mo K α radiation. Final unit cell dimensions were obtained and refined on an entire data set. Structures were solved by direct methods using the SHELX-97 program package¹⁶ and refined with the full-matrix least-squares method with anisotropic thermal parameters for the non-hydrogen atoms. Cu(II) atom in 1 resides on a 2-fold axis in space group $C2/c$, and the coordinated sulfate anion is disordered around this axis with equal probabilities together with the H-bonded methanol solvent molecule. Attempts to refine the structure in noncentrosymmetric space group Cc taking in account possible merohedral twinning do not improve the convergence of refinement, and the sulfate anion remained disordered. The sulfate anion in 2 was also found to be disordered over two positions with 0.648(14) and 0.352(14) occupancies, although the complex occupies the general position in the structure. In all structures the C(sp²)-bound H atoms were placed in calculated positions and treated using a riding model approximation with $U_{iso}(\text{H}) = 1.2U_{eq}(\text{C})$; H atoms of the methyl groups were found and refined using AFIX 137 instruction and $U_{iso}(\text{H}) = 1.5U_{eq}(\text{C})$, while the O-bound H atoms were found from differential Fourier maps at intermediate stages of the refinement, and their positions

were constrained using the AFIX 83 instruction in SHELXL for the hydroxyl group in the methanol molecule in 1 and restrained using DFIX instruction for water molecules. These hydrogen atoms were refined with isotropic displacement parameter $U_{iso}(\text{H}) = 1.5U_{eq}(\text{O})$. Figures were produced using Mercury.¹⁷ X-ray data and details of the refinement for 1–3 are summarized in Table 1; selected geometric parameters and the hydrogen-bonding geometry are given in Tables 1S and 2S, Supporting Information.

Table 1. Crystal and Structure Refinement Data for 1–3

compound	1	2	3
empirical formula	C ₂₅ H ₂₀ N ₄ O ₅ SCu	C ₂₇ H ₂₇ N ₅ O ₇ SCu	C ₂₄ H ₂₆ N ₄ O ₉ SCu
fw	552.05	629.14	610.09
cryst syst	monoclinic	monoclinic	triclinic
space group	$C2/c$	$P2_1/c$	$P-1$
Z	4	4	2
a (Å)	17.4130(9)	10.9173(4)	9.4270(4)
b (Å)	11.9040(4)	16.9660(7)	11.7082(6)
c (Å)	12.4308(7)	14.9508(8)	12.6902(5)
α (deg)	90	90	63.470(4)
β (deg)	117.491(7)	100.164(5)	89.255(3)
γ (deg)	90	90	86.845(4)
V (Å ³)	2285.8(2)	2725.8(2)	1251.17(10)
D_{calcd} (g cm ^{−3})	1.604	1.533	1.619
μ (mm ^{−1})	1.094	0.934	1.019
F(000)	1132	1300	630
no. of reflns collected/unique	4060/2224	9752/5321	8721/4623
no. of reflns with [$I > 2\sigma(I)$]	1682	2914	3957
data/restraints/parameter	2224/35/196	5321/21/463	4623/0/382
goodness-of-fit (GOF) on F^2	1.001	0.998	1.003
R1, $wR2$ [$I > 2\sigma(I)$]	0.0451, 0.1103	0.0645, 0.0770	0.0385, 0.0954
R1, $wR2$ (all data)	0.0657, 0.1240	0.1330, 0.0913	0.0480, 0.1019
$\Delta\rho_{\text{max}}, \Delta\rho_{\text{min}}$ (eÅ ^{−3})	0.363, −0.299	0.512, −0.515	0.349, −0.311

Computational Methods. The molecular geometries of the free *phen* molecule (Refcode OPENAN)¹⁸ and ionic complex 3 were taken from experimental X-ray data and reoptimized for the ground and excited state with DFT and TD-DFT methods, respectively (at M06-QX/SDD theory level). All calculations were performed using the Gaussian 2009 suite of programs.¹⁹ Density functional theory (DFT) with the M05-QX exchange-correlation functional and SDD effective core potential and D95 basis set²⁰ were used for geometry optimization of the *phen* free molecule and complex 3. The M05-QX functional (also known as M05-11/4X) was derived²¹ by interpolation between M05 and M05-2X functionals²² to include 35% of the exact exchange. We chose to use this functional as it more accurately predicts the energies of the electronic states with higher charge transfer character when compared to the more commonly used functionals (such as B3LYP). It was repeatedly shown to improve the description of both the lowest and the higher excited states in polar

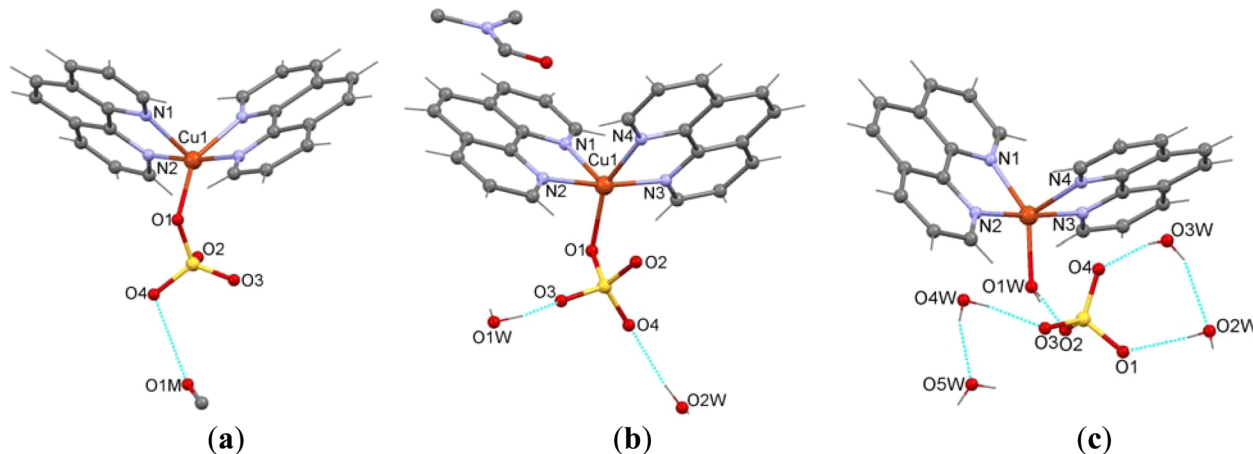


Figure 1. Molecular structures of **1** (a), **2** (b), and **3** (c). H atoms in methanol and *dmf* molecules are omitted for clarity.

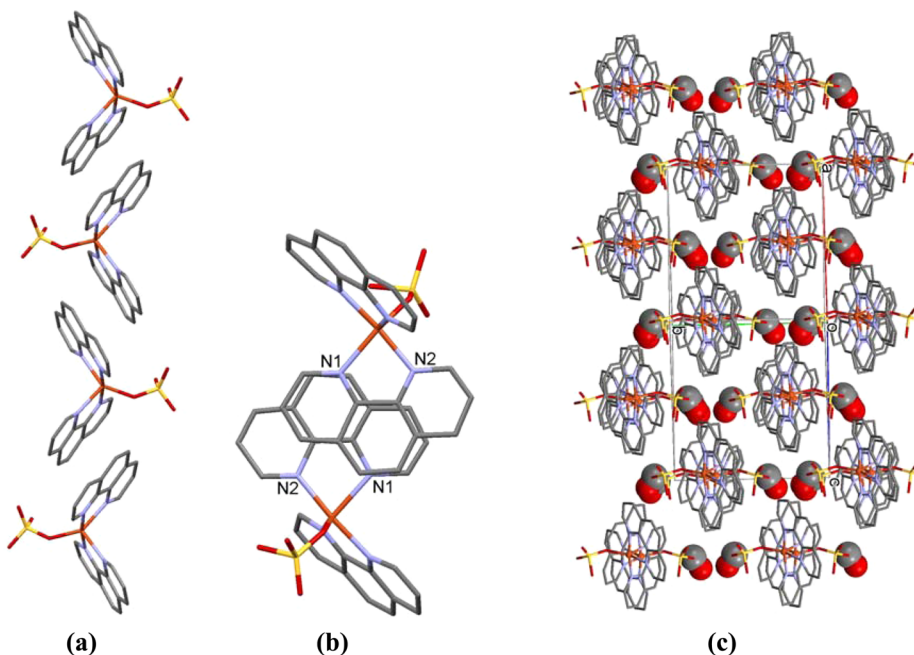


Figure 2. Crystal packing patterns in **1**. (a) Tape of the complexes supported by $\pi-\pi$ stacking interactions along the [101] direction. (b) Manner of *phen* overlapping; view perpendicular to the plane of the overlapping *phen* ligands. (c) Enclathration of methanol molecules in the crystal lattice. H atoms omitted for clarity. Methanol molecules are shown in space-filling mode.

chromophores.^{23–26} The basis set with no diffusion functions was chosen in order to prevent the artificial Rydberg contributions into the valent excited states, as described in refs 27 and 28. Time-dependent density functional theory (TD-DFT)²⁹ in the Tamm–Dancoff approximation (TDA)³⁰ was used to describe the excited states. The full TD-DFT, unlike TD-DFT, incorrectly predicted some triplets to be more stable than the ground state and was not used here for this reason. Vertical absorption and emission spectra were predicted using the optimized ground and excited state geometry, respectively. The polarizable continuum model (PCM)³¹ with a dielectric constant of $\epsilon = 9$ was employed to account for the DCM solvent or crystalline environment.

RESULTS AND DISCUSSION

Structural Studies. Mononuclear compounds **1–3** were obtained similarly by mixing the starting components copper(II) sulfate monohydrate and 1,10-phenanthroline in different

solvents, methanol for **1**, a water:methanol:*dmf* mixture in a 1:2:1 molar ratio for **2**, and a water:methanol mixture in a 1:3 molar ratio for **3** followed by boiling the reaction mixtures, simultaneous cooling, and precipitation of the studied compounds. The reported examples demonstrate the easy solvent/anion exchange that is justified by separation of different complexes from approximately the same synthetic conditions.

A survey of the CSD (CSD version 5.35, Nov 2013) revealed about 10 hits that comprise the Cu(II) cation, *phen* ligand, sulfate anion, and different solvent molecules. Among them one, catena($(\mu_2\text{-sulfato-O,O}')$ -diaqua-(*phen*)—copper(II)),³² represents a one-dimensional coordination polymer and one, bis($(\mu_3\text{-hydroxo})-(\mu_2\text{-hydroxy})$)-diaqua-tetrakis(*phen*)-tetra-copper disulfate octahydrate, represents the tetranuclear cluster,³³ while all others represent mononuclear solids with different solvent/guest molecules encapsulated in the crystal lattices.^{34–39} Newly synthesized compounds **1–3** differ by the

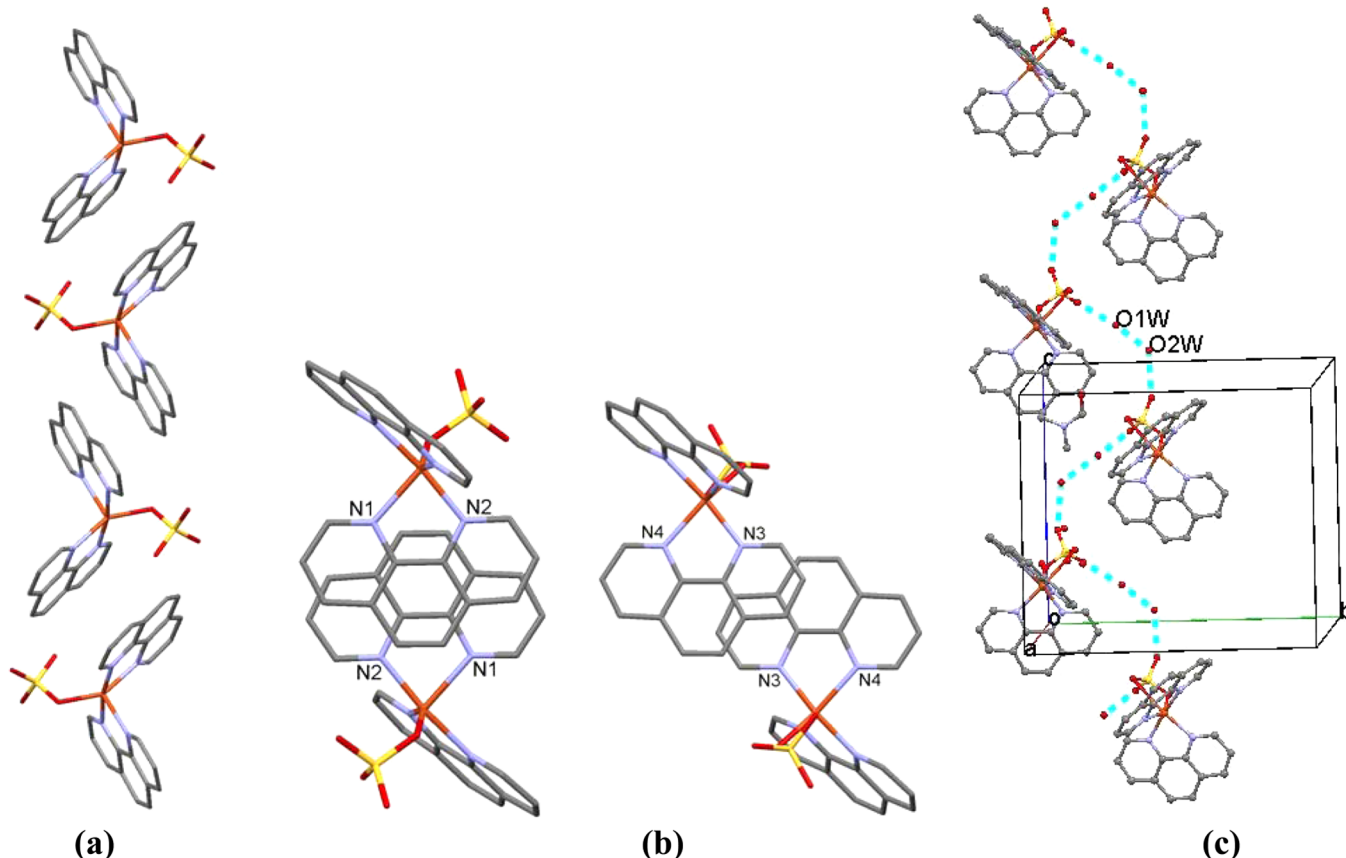


Figure 3. Crystal packing patterns in **2**. (a) Tape of the complexes supported by π - π stacking interactions. (b) Two modes of *phen* overlapping; view perpendicular to the plane of the overlapping *phen* ligands. (c) Enclathration of water molecules in the crystal lattice. H atoms omitted for clarity.

Cu(II) first and second coordination spheres as evidenced from the general views of the complexes shown in Figure 1. Similar to the reported data,^{34–38} **1** (Figure 1a) and **2** (Figure 1b) represent the neutral molecular species with the sulfate anion coordinated to the metal center while **3** (Figure 1c) represents the ionic structure composed of the complex cations $[\text{Cu}(\text{phen})_2\text{H}_2\text{O}]^{2+}$ and outer-sphere sulfate anions. In all structures the N_4O surrounding the metal may be described as intermediate between distorted square pyramidal with the most distant from the metal nitrogen atom in the apical position and distorted trigonal bipyramidal where two proximate nitrogen atoms are axial (Table 1S, Supporting Information). The degree of distortion is indicated by the general descriptor $\tau = (\beta - \alpha)/60$ for five-coordinated complexes,^{40–42} where α and β are the two largest angles at the metal center. For the idealized square pyramid and trigonal bipyramidal extremes $\tau = 0$ and 1, respectively. In the studied complexes τ equals 0.430 for **1**, 0.339 for **2**, and 0.538 for **3**. The sulfate anion coordinates in a monodentate mode in **1** and **2**, the Cu–O distance is 1.901(4) and 2.006(8) Å and Cu(1)–O(1)–S(1) angle 130.6° and 110.1(6)° and the coordinated water molecule in **3** is situated 1.979(2) Å from the Cu(II) atom. The twisted shape of the molecular complexes **1** and **2** and the complex cation in **3** is characterized by the dihedral angles between the chelate *phen* ligands of 68.90°, 73.31°, and 76.77° in **1**, **2**, and **3**, respectively.

Comparison of the crystal packing in **1–3** with the related reported compounds has been undertaken to estimate the dominate supramolecular patterns and analyze the mode of

enclathration of different solvents in the crystal lattice. In **1** the methanol molecule is attached to the sulfate anion via a single OH···O hydrogen bond: O···O 2.84(1) Å, angle OHO 170° (Figure 1a, Table 2S, Supporting Information). This is the strongest intermolecular interaction in this solid. The crystal packing of these two-component H-bonded entities is governed by the stacking interactions between the *phen* moieties from the $[\text{Cu}(\text{phen})_2\text{SO}_4]$ complexes related by the inversion centers. The generated stacking patterns, identical for both *phen* ligands due to the C_2 symmetry of the molecular complex, result in rod-like aggregates along the [101] direction (Figure 2a). The separations between the centroids of the overlapping rings of 3.538 Å (Figure 2b) and the interplanar separation of 3.498 Å indicate the face-to-face stacking.^{43–45} The metal···metal separation through the stacked ligands is 8.070(3) Å. Figure 2c demonstrates the mode of enclathration of methanol molecules in the crystal lattice.

Inspection of the reported data for the landscape of mononuclear complexes $\{[\text{Cu}(\text{phen})_2(\text{SO}_4)] \text{ solv}\}$ (solv = methanol, ethanol, ethane-1,2-diol, propane-1,3-diol, propane-1,2-diol, butane-2,3-diol),^{34–38} where complex **1** represents the first missing member, reveals their isomorphic character indicated by preservation of the crystal symmetry (monoclinic, C) with the proportional increase of the unit cell dimensions, in favor of the robustness of the *phen* embracing^{46,47} in the absence of other stronger interactions and the possibility of accommodation of alcohol molecules close in structure and size in the alike crystal lattices.

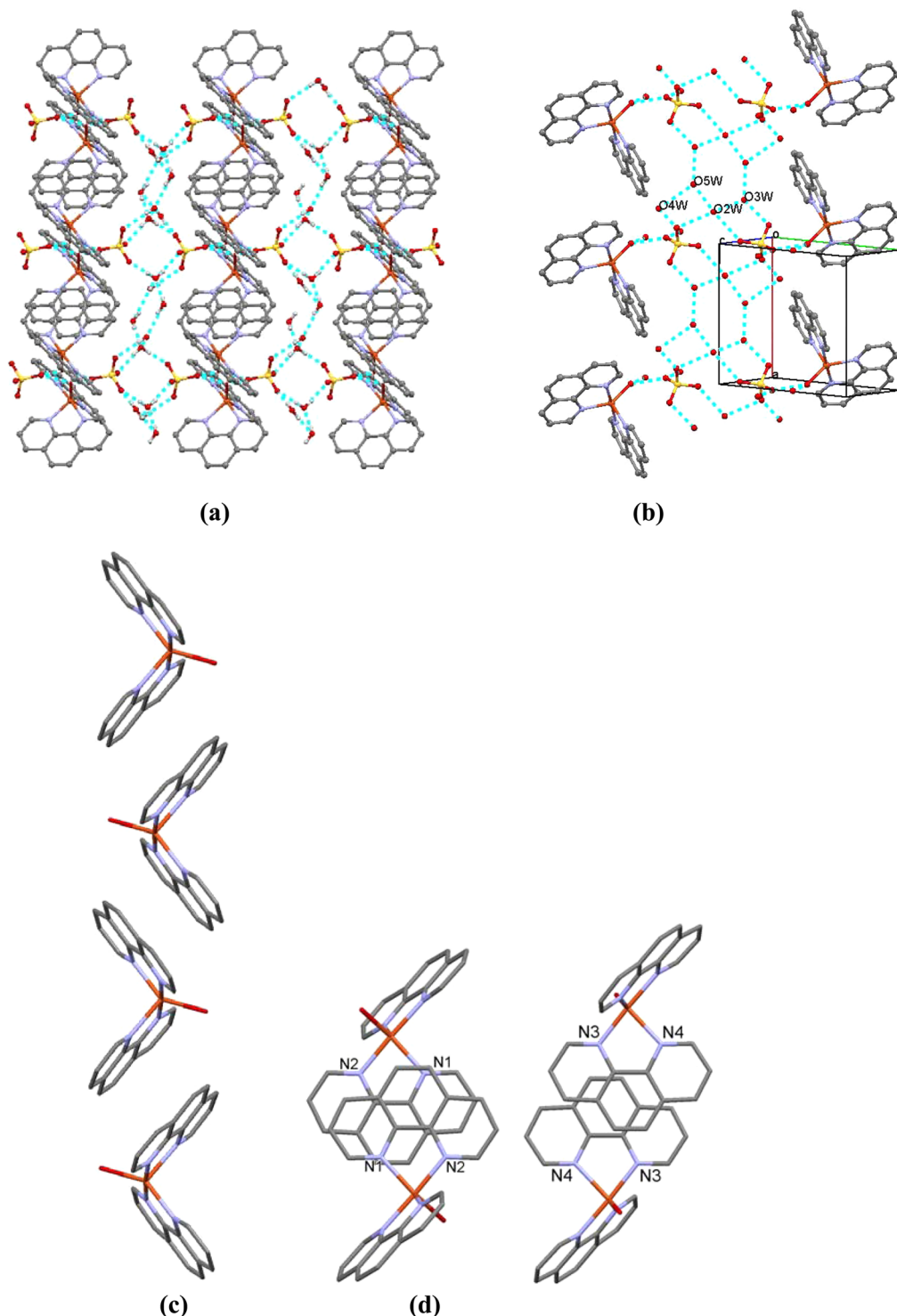


Figure 4. Crystal packing patterns in 3. (a) Cationic $[Cu(phen)_2H_2O]^{2+}$ moieties embedded in the hydrophilic network. (b) View of H-bonded ribbon composed of water molecules and sulfate anions. (c) Cationic tape supported by $\pi-\pi$ stacking interactions. (d) Two modes of *phen* overlapping; view perpendicular to the plane of the overlapping *phen* ligands.

The crystallization of **2** from the water–DMF solvent mixture is accompanied by accommodation of protic water and aprotic DMF molecules. The crystal structure of **2** reveals that $[Cu(phen)_2SO_4]$ complexes reside in general positions in the primitive monoclinic unit cell and aggregate in rod-like structure by stacking interactions again (Figure 3a), although the manner of overlapping differs from **1** (Figure 3b). The *phen* ligands (identified by N(1) and N(2) atoms) are related by an

inversion center overlapping by only the central phenyl moiety with an interplanar separation of 3.420 Å and a centroid…centroid distance of 3.467 Å (face to face stacking), while for the other pair of *phen* ligands (identified by N(3) and N(4) atoms) related by the center of symmetry, again, overlap occurs between two rings with an interplanar separation 3.300 Å and centroid…centroid distances of 3.707 and 3.809 Å for pyridine…pyridine and pyridine…phenyl pairs, respectively,

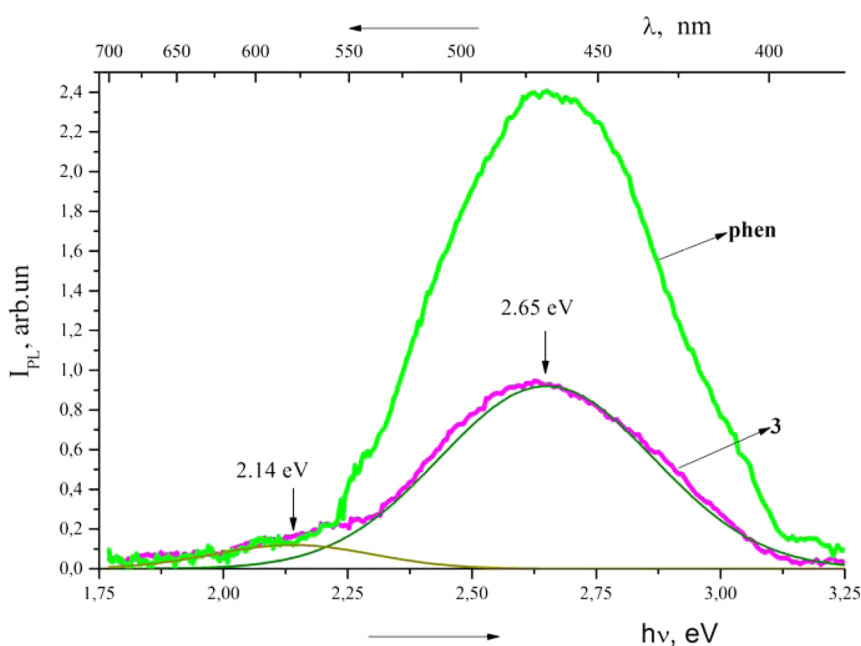


Figure 5. Emission spectra for **3** and free *phen* measured in the solid state.

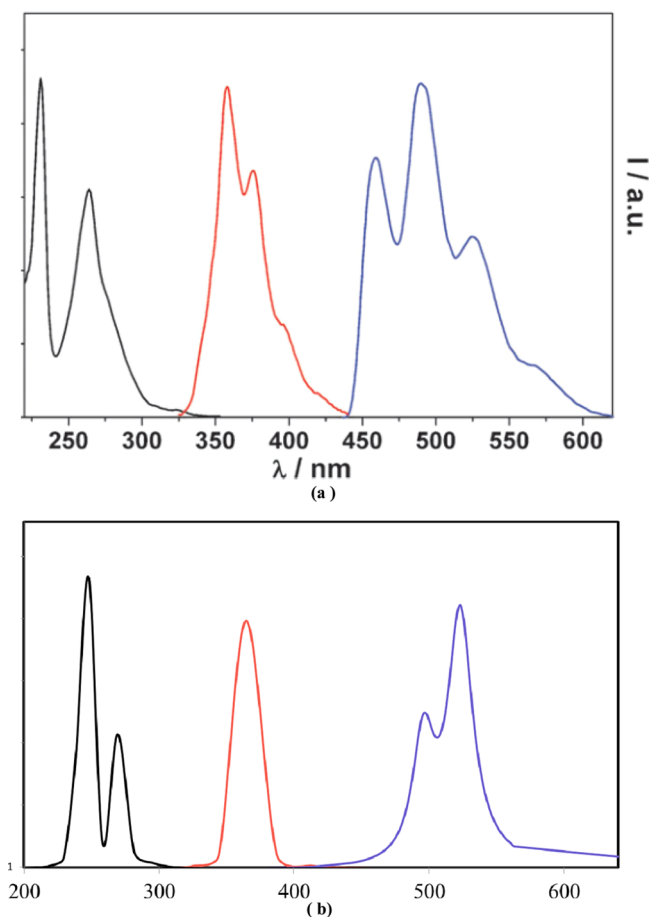


Figure 6. Solution electronic spectra of *phen*: absorption (black), fluorescence (red), and phosphorescence (blue). (a) Experimental results (adopted from ref 53) and (b) predicted in this work.

thus indicating the slipping stacking interaction with offset.^{43,45} The consecutive metal···metal separations through the stacked ligands insignificantly differ now, being equal to 8.4555(9) and

8.7711(9) Å. The outer-sphere two-membered water clusters alternate with the sulfate anions, giving rise to the infinite helical H-bonded motifs (Figure 3c, Table 2S, Supporting Information) and modifying the stacking patterns fixed in **1**. Aprotic planar DMF molecules are in the hydrophobic regions without specific intermolecular interactions.

Elimination of the sulfate anion from the Cu(II) coordination core in **3** accompanied by the increased number of water molecules including that coordinated to the Cu(II) atom results in the continuous anionic hydrophilic areas (Figure 4a) which accumulate the mononuclear aqua dications. The hydrophilic regions in **3** represent the ribbon motifs composed of the circular H-bonded patterns⁴⁸ that include the centrosymmetric six-membered water cluster, $R_6^4(12)$ [O(5w), O(2w), O(3w)], and centric and acentric water–anion aggregates formulated as the circular motifs, $R_4^2(8)$ [O(1w), SO_4^{2-}], $R_3^3(6)$ [O(2w), O(3w), SO_4^{2-}], $R_4^4(14)$ [O(2w), SO_4^{2-}], $R_4^3(8)$ [O(2w), O(5w), O(4w), SO_4^{2-}]. Water inclusion occurs in the DD [O(1w), O(4w)], DDA [O(3w), O(5w)], and DDAA [O(2w)] modes (Figure 4b). Despite the crucial impact of the hydrogen bonding on crystal stabilization, this particular solid also demonstrates the preservation of the stacking patterns between the inversion-related chelate *phen* moieties (Figure 4c and 4d). Inspection of crystal packing in **3** discloses a packing motif analogous to that in **1** and **2**, notwithstanding the cationic nature of $[Cu(phen)_2H_2O]^{2+}$ units. The cationic stacking rods are parallel to the [1 1 -1] direction. The interplanar separation of *phen* ligands (N1, N2) in the centrosymmetric pattern with overlapping of all three rings is 3.477 Å, and centroid···centroid distances are 3.741, 3.666, and 3.822 Å for pyridine···pyridine, pyridine···phenyl, and phenyl···phenyl pairs, respectively, thus indicating the slipping stacking interaction with offset. For the second *phen* ligand (N3, N4) in the centrosymmetric dimer the interplanar separation is 3.330 Å, and centroid···centroid distances are 3.798 and 3.548 Å for pyridine···phenyl and phenyl···phenyl pairs, respectively. These parameters also indicate a stacking interaction with offset. The corresponding metal···metal separations through the stacked

Table 2. Lowest Excited States for *phen* Free Ligand in the Ground (vertical absorption) and Relaxed Excited State Geometries Optimized with Various Symmetry Constraints: Excitation Energy, Wavelengths, Oscillator Strengths, and Leading Configurations (HOMO–LUMO is H–L etc.)

state	vertical, C_{2v}			leading config.	type	relaxed, C_{2v}		relaxed, C_s		relaxed, C_1	
	E_{ex} eV	λ , nm	osc.			E_{ex} eV	λ , nm	E_{ex} eV	λ , nm	E_{ex} eV	λ , nm
1^1A_2	4.10	302	0.000	H1–L1	$n-\pi^*$	3.40	365	3.40	365	3.21	386
1^1B_1	4.19	296	0.008	H1–L	$n-\pi^*$	3.47	357				
1^1A_1	4.36	285	0.002	H–L1	$\pi-\pi^*$	4.03	307				
1^1B_2	4.57	271	0.305	H–L	$\pi-\pi^*$	3.89	318	3.83	323		
2^1B_1	4.65	266	0.006	H3–L1	$n-\pi^*$	3.98	311				
2^1A_2	4.66	266	0.000	H3–L	$n-\pi^*$	3.95	314				
2^1B_2	5.03	247	1.555	H2–L1	$\pi-\pi^*$	4.80	258				
2^1A_1	5.19	239	0.341	H2–L	$\pi-\pi^*$	4.95	250				
1^3B_2	3.10	399		H–L	$\pi-\pi^*$	2.99	528	2.35	527	2.50	496
1^3A_2	3.55	348		H1–L1	$n-\pi^*$	2.95	420	2.77	448	2.37	523
1^3B_1	3.71	333		H1–L	$n-\pi^*$	3.23	384				
1^3A_1	3.74	331		H–L1	$\pi-\pi^*$	3.25	381				

ligands significantly differ now being equal to 7.4214(6) (N1, N2) and 8.9695(6) Å (N3, N4).

Photoluminescence Properties. The design of Cu(II) sensors remains a focus of synthetic chemists due to the vital role of this metal in physiological and environmental processes.^{2,49,50} The Cu(II) quenching of fluorescence by mechanisms inherent to paramagnetic species is documented.^{49–52} The paramagnetic Cu(II) cation with an incomplete d shell can quench the fluorescence of the fluorophore near it via electron or energy transfer.^{51,52}

Although a spectral study of complexes **1** and **2** was not possible due to the poor crystal quality, emission spectra of the crystalline *phen* ligand and complex **3** were recorded in the solid state at room temperature. The corresponding plots are shown in Figure 5. Both compounds display a broad band with a maximum at 2.65 eV (470 nm) that can be assigned to the *phen* emission. This band demonstrates a 3-fold intensity decrease for the complex against the free *phen* molecule. Gaussian deconvolution analysis reveals a minor component in the emission spectra of both compounds centered at 2.14 eV (580 nm).

The photophysics of the *phen* ligand and its complexes in solutions is well documented.⁵³ The free ligand in DCM solution at room temperature is characterized by 310 nm fluorescence with a quantum yield of 0.0087 and a short singlet lifetime of 1 ns. At 77 K an intense phosphorescence band at 489 nm with a long triplet lifetime (1.1 s) is also detected.⁵⁴ Detailed analysis revealed two close-lying excited states, $n-\pi^*$ and $\pi-\pi^*$, that may switch order depending on solvent polarity.⁵⁵

While complexation with reducing metal cations (such as Ru(II)) enables formation of low-energy metal-to-ligand charge-transfer electronic states, the metal cations that are hard to oxidize (e.g., Zn(II) and Ag(I)) form complexes that exhibit absorption and emission spectra which are assigned to the *phen* moieties, weakly perturbed compared to the free ligands under the same conditions.⁵⁶ Specifically, the substituted *bis-phen* complex of Ag(I) exhibits a low-temperature phosphorescence at 495 nm, while its Zn(II) analog emits fluorescence at 455 nm.⁵⁷ Generally speaking, metal-to-ligand transitions in Cu(II) complexes are located much higher in energy, but metal-centered d–d electronic transitions can cause relatively intense absorption bands in the visible spectral window. The lowest metal-centered excited states are located in

the near-infrared region and do not appear on the emission spectra (as they deactivate via ultrafast nonradiative processes).⁵⁸ Ligand-centered excited states can also deactivate via this mechanism. For this reason, relatively few reports on the emission of Cu(II) complexes with the *phen* ligand have been published, Figure 6. However, it was reported that cation $[\text{Cu}(\text{phen})_2\text{N}_3]^+$ with the metal in a distorted trigonal bipyramidal coordination geometry exhibits fluorescence at 350 nm.⁵⁹ Another example is dinuclear complex $[\text{Cu}_2(\text{phen})_2(\text{H}_2\text{O})_4(\text{cbtc})]$ (cbtc = 1,2,3,4-cyclobutanetetracarboxylate tetraanion) that has strong fluorescence at 358 nm.⁶⁰ On the basis of this information, we can preliminarily assign the emission observed from **3** in the 470–600 nm range as phosphorescence emitted by the ligand-centered triplet state.

In order to analyze this emission signal with greater detail we performed calculations using density functional theory (DFT) and the Tamm–Dancoff approximation to time-dependent density functional theory (TDA-DFT). The DFT approach was widely shown to make an accurate prediction of the structure and properties for the molecules and solids, such as aggregation and crystal formation,^{23,61–63} reaction rates and mechanisms,^{24,64–66} and linear and nonlinear optical properties.^{25,67–69}

The ground state singlet geometry for the *phen* molecule was optimized in the C_{2v} point group, and the lowest vertical excitations in this geometry are listed in Table 2 (column 2). The leading electronic configurations are reported in Table 2 (column 5) and illustrated with Kohn–Sham orbitals in Figure 7. Among these essential orbitals most are of π and π^* type, and only two are of n type. These two represent symmetric (HOMO-1, or H1) and antisymmetric (HOMO-3, or H3) linear combinations of the lone pairs on the nitrogen atoms. One can see from Table 2 that singlet $\pi-\pi^*$ states can be separated into two pairs of nearly degenerate 1^1A_1 and 1^1B_2 states. Three of them have large oscillator strengths (“bright” states) and are responsible for the two bands on the absorption spectrum (270 and 240 nm in Figure 6b). However, the lowest among the excited singlet states are dark $n-\pi^*$ states that also form a pair (1^1A_2 and 1^1B_1). Geometry relaxation of each individual state with symmetry constraint results in some stabilization (Table 2, column 7), while states retain their identity. When we lift the symmetry constraints but enforce molecular planarity (Table 2, column 9), the lowest $n-\pi^*$ singlet becomes localized on one of two nitrogen lone pairs

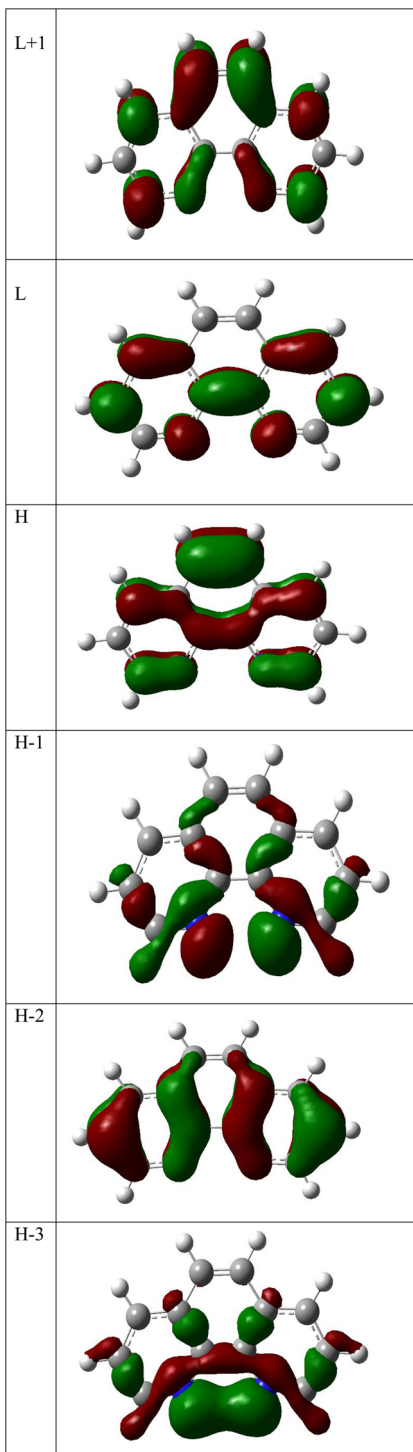


Figure 7. Essential Kohn–Sham orbitals in the ground state *phen* geometry.

(instead of symmetric and antisymmetric combination of the two lone pairs), but its excitation energy changes insignificantly. More importantly, the $\pi-\pi^*$ state relaxes to 3.83 eV (323 nm). At this optimum geometry it becomes nearly degenerate with the lowest $n-\pi^*$ state, which indicates the close proximity of their conical intersection and, hence, the fast internal conversion between them. If $\pi-\pi^*$ state was the lowest singlet in its relaxed geometry (metastable minimum on potential surface, separated from the conical intersection by sizable potential barrier), one would expect dual fluorescence from

Table 3. Lowest Excited States for $[\text{Cu}(\text{phen})_2 \cdot \text{H}_2\text{O}]^{2+}$ Complex in the Ground and Relaxed Excited State Geometries

state	vertical, C_2			type	relaxed, C_1		
	$E_{\text{ex}} \text{ eV}$	$\lambda, \text{ nm}$	leading configurations		$E_{\text{ex}} \text{ eV}$	$\lambda, \text{ nm}$	
1 ² A	0.89	1385	$\beta\text{HS-L}$	d-d			
1 ² B	0.93	1336	$\beta\text{H4-L}$	d-d			
2 ² A	1.00	1235	$\beta\text{H15-L}$	d-d			
2 ² B	1.09	1139	$\beta\text{H13-L}$	d-d			
1 ⁴ B	2.46	504	$\alpha\text{H-L2}, \beta\text{H-L3}$	$\pi-\pi^*$	2.45	506	
1 ⁴ A	2.46	504	$\alpha\text{H1-L2}, \beta\text{H1-L3}$	$\pi-\pi^*$			
2 ⁴ A	3.19	388	$\alpha\text{H1-L}, \beta\text{H1-L1}$	$\pi-\pi^*$			
2 ⁴ B	3.20	387	$\alpha\text{H-L}, \beta\text{H-L1}$	$\pi-\pi^*$			
3 ⁴ B	3.53	351	$\alpha\text{H2-L}, \beta\text{H2-L1}$	$\pi-\pi^*$			
3 ⁴ A	3.53	351	$\alpha\text{H3-L}, \beta\text{H3-L1}$	$\pi-\pi^*$			
3 ² A	3.58	346	$\beta\text{H1-L}$	$\pi-d$			
3 ² B	3.60	344	$\beta\text{H-L}$	$\pi-d$			
4 ⁴ B	3.91	317	$\alpha\text{H2-L2}, \beta\text{H2-L3}$	$\pi-\pi^*$			
4 ⁴ A	3.91	317	$\alpha\text{H3-L2}, \beta\text{H3-L3}$	$\pi-\pi^*$			
4 ² B	3.95	314	$\beta\text{H2-L}$	$\pi-d$			
4 ² A	3.96	313	$\beta\text{H3-L}$	$\pi-d$			
5 ⁴ A	4.28	290	$\alpha\text{H4-L}$	$n-\pi^*$	2.25	552	
5 ⁴ B	4.33	286	$\alpha\text{H4-L1}$	$n-\pi^*$			

$\pi-\pi^*$ and $n-\pi^*$ excited singlet states.^{70,71} However, this is not the case here, and the double peak on the fluorescence spectrum (Figure 6a) clearly has vibronic structure. When the molecular planarity constraint is lifted, these states mix and relax to an excitation of 3.21 eV (386 nm), which is relatively dark (its oscillator strength is 0.004). This explains the long fluorescence lifetime and predominant de-excitation by non-radiative channels (low fluorescence quantum yield). One of these channels may be intersystem crossing to a triplet state that is lower in energy.

Next, let us consider the triplet excitations also reported in Table 2 (bottom). This time the HOMO–LUMO transition (abbreviated H–L in Table 2) is of $\pi-\pi^*$ nature. It is lowest at 3.10 eV, and $n-\pi^*$ is a distant second at 3.55 eV. Geometry optimization under symmetry constraint (Table 2, column 7) brings the ${}^3\text{A}_2$ state of $n-\pi^*$ nature to 2.95 eV, where it is the lowest energy triplet, and the ${}^3\text{B}_2$ state of $\pi-\pi^*$ nature is more than 1 kcal/mol higher in energy. When the symmetry is distorted to preserve only molecular planarity (Table 2, column 9), both $\pi-\pi^*$ and $n-\pi^*$ triplet states relax to 2.35 (527 nm) and 2.77 eV (448 nm). Each of these states is the lowest energy excitation in its respective optimized geometry. Removal of all symmetry constraints (Table 2, column 11) results in further stabilization. While the vertical emission energies of these $n-\pi^*$ and $\pi-\pi^*$ triplets is distinctly different (496 and 523 nm), the difference in their total energies becomes less than 0.5 kcal/mol and allows for comparable equilibrium populations of these potential minima so that both emission wavelengths can be observed. Prediction of the brightness of the triplet emission requires calculation of the spin–orbit coupling matrix elements, which extends beyond the scope of this work. Therefore, our calculations predict two phosphorescence bands from *phen* in DCM solution, which is in close agreement with Figure 6 and approximately corresponds to the dual emission we report in Figure 5 (wavelengths being somewhat perturbed by $\pi-\pi$ -stacking interactions, however).

Finally, we will consider the excited states of the complex $[\text{Cu}(\text{phen})_2 \cdot \text{H}_2\text{O}]^{2+}$, reported in Table 3 and illustrated with

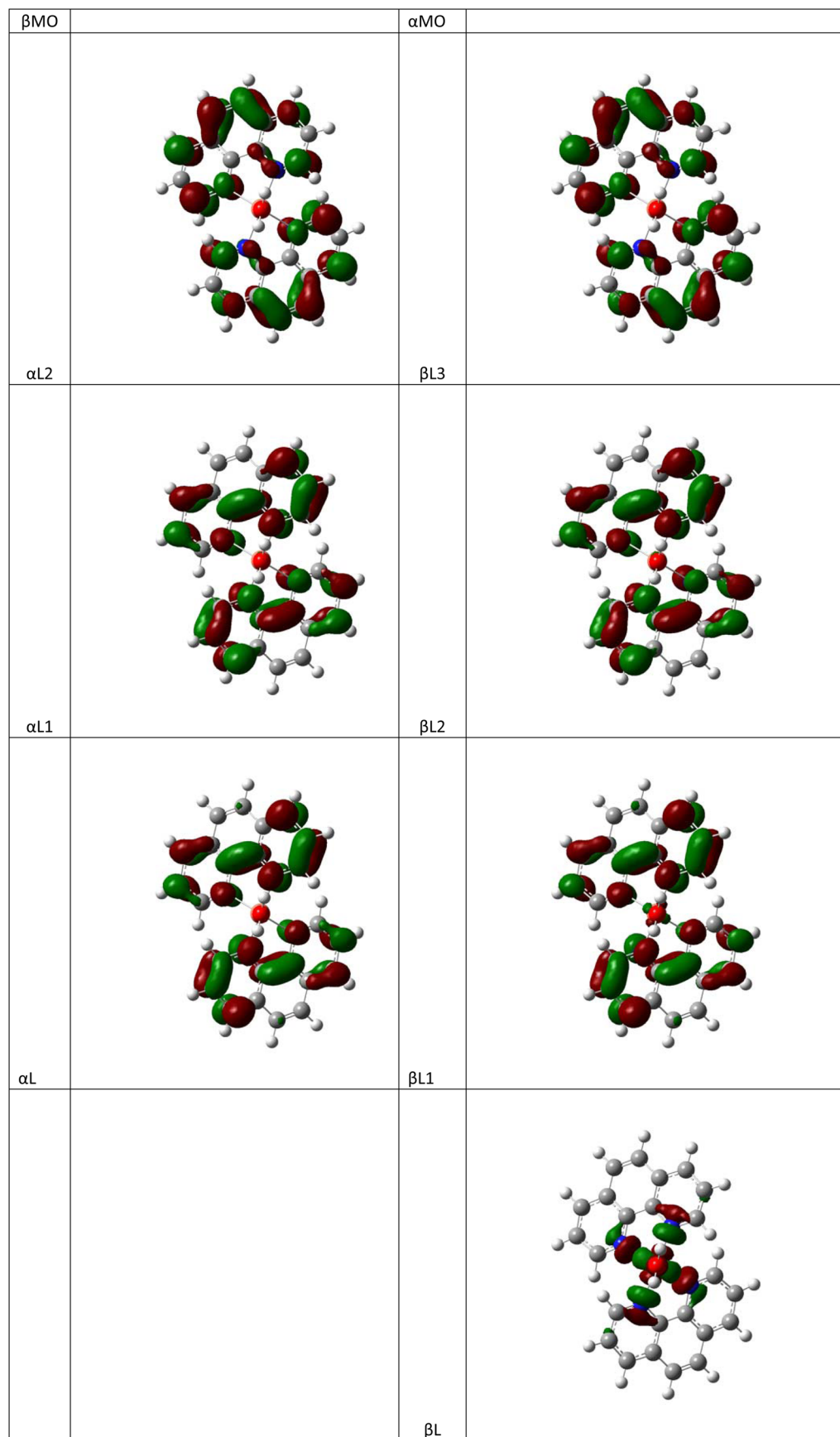


Figure 8. continued

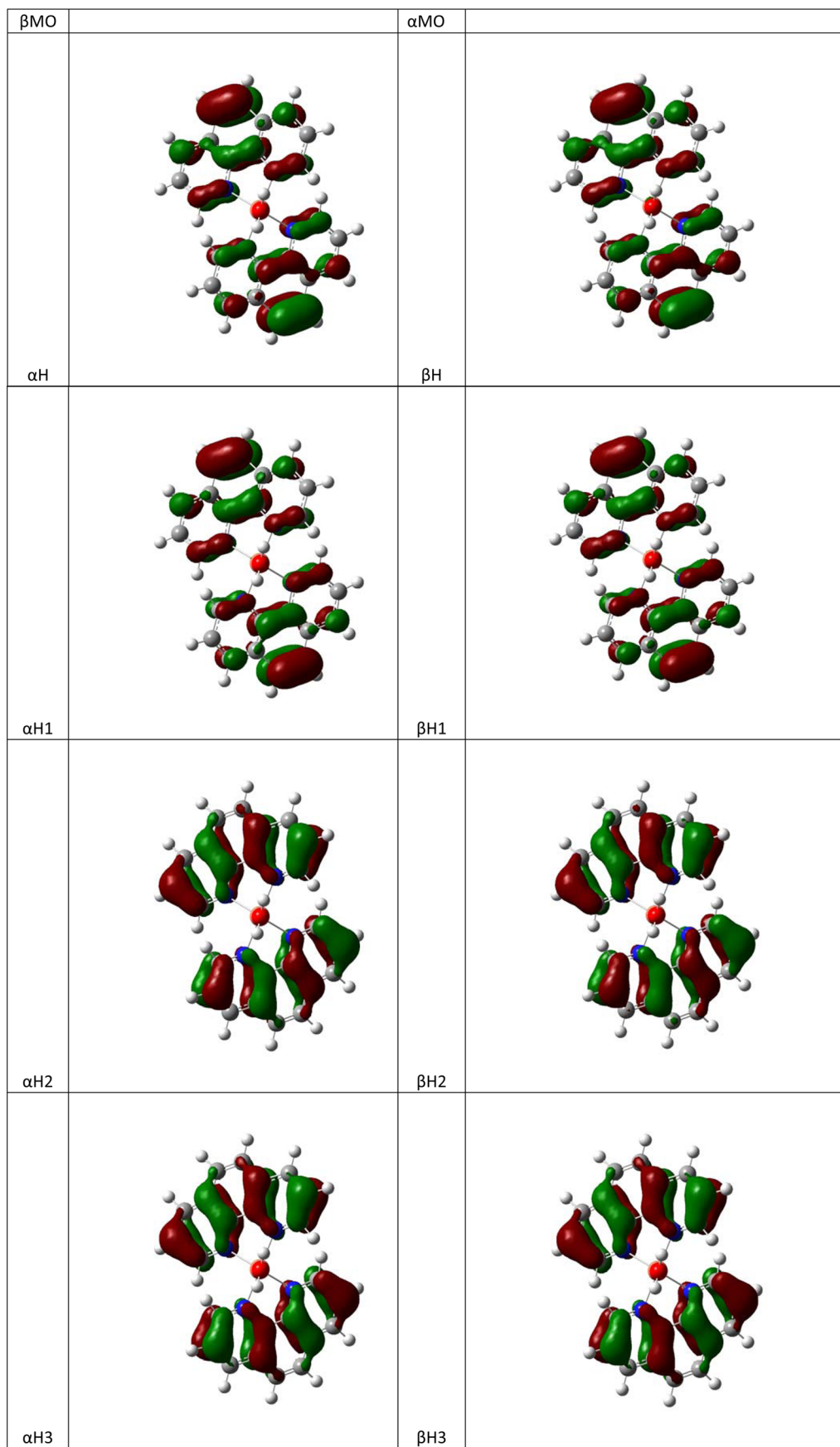


Figure 8. continued

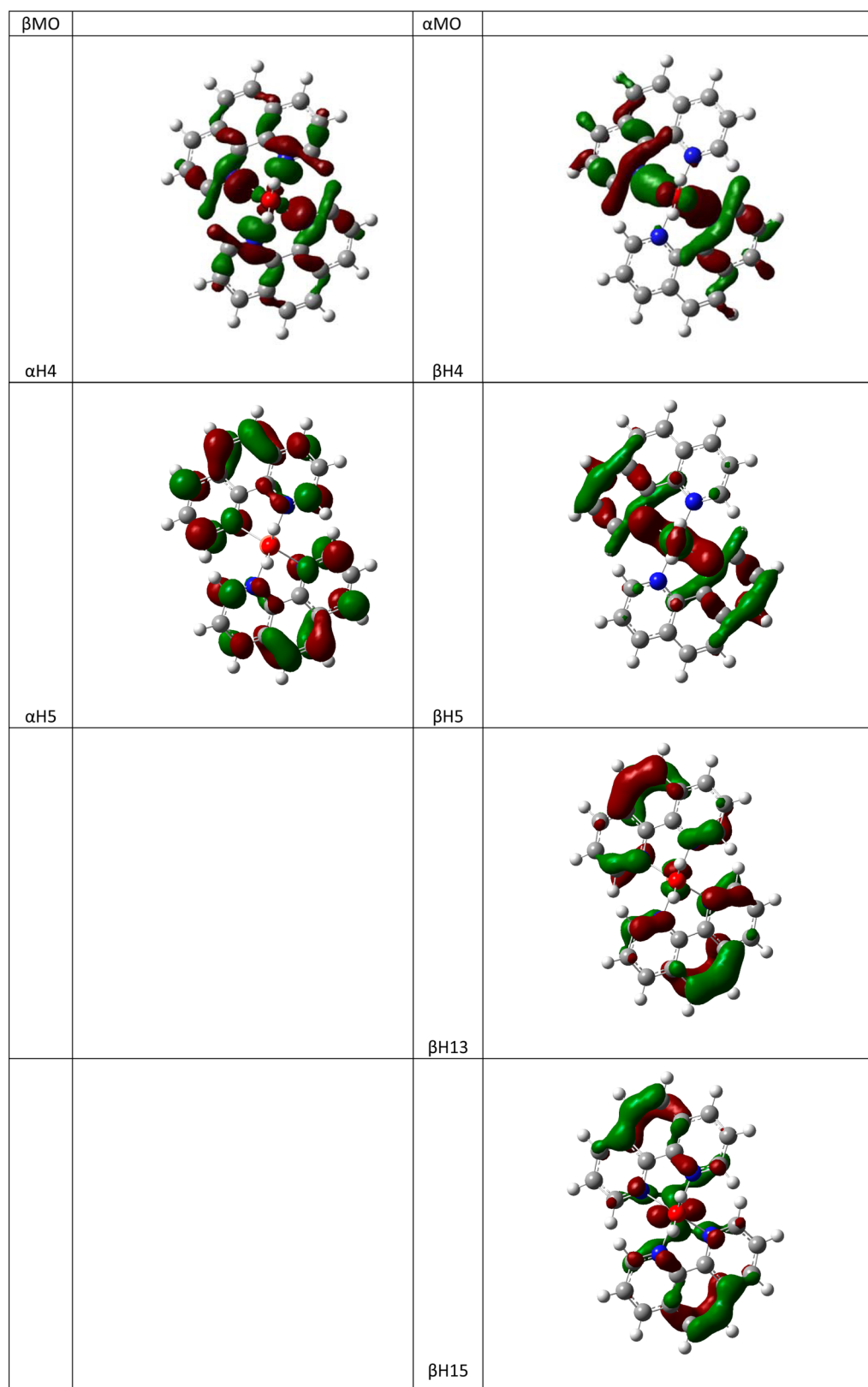


Figure 8. Essential Kohn–Sham orbitals in C_2 -optimized complex $[\text{Cu}(\text{phen})_2 \cdot \text{H}_2\text{O}]^{2+}$.

Kohn–Sham orbitals gathered in Figure 8. Since the central Cu(II) ion has 9 electrons in its d level, the ground state of this complex is a doublet. The four lowest excited states (with an excitation energy close to 1 eV) are also doublets, corresponding to localization of the hole on the other d

orbitals. The higher states are eight quadruplets (ligand-centered triplet excitations) and four doublets (metal to ligand charge transfer states). The two quadruplets, corresponding to the ligand-centered $n-\pi^*$ triplet excitations, appear only at 4.3 eV (290 nm). However, geometry relaxation with no symmetry

constraints results in elongation for one of the axial Cu–N bonds from 1.98 to 2.16 Å, and the vertical emission energy is reduced to 2.25 eV (552 nm). The $\pi-\pi^*$ quadruplet, on the other hand, remains at 2.45 eV (506 nm) after its geometry optimization. Thus, phosphorescence wavelengths predicted for the complex (552 and 506 nm) are similar to those predicted for the free ligand (523 and 496 nm) and in qualitative agreement with the dual-emission measurements (Figure 5). The presence of the d–d excited states close to 1 eV in the complex opens new channels for nonradiative decay and may explain partial emission quenching observed in the complex as compared to the free ligand. Another possible mechanism for phosphorescence quenching is an intermolecular stacking interaction.

The excited states of two interacting chromophores is split in such a way that in a face-to-face stack (so-called H-aggregate) in the lower energy combination the transition dipoles cancel and in the higher energy one the transition dipoles double. This results in a blue shift of the absorption band and complete fluorescence quenching.⁷² For the head-to-tail arrangement of the chromophores (J aggregate) the state coupling is opposite, so that absorption is red shifted and fluorescence is super-radiant. In realistic dimers and crystals these extremes occur rarely, but subradiance associated with the overlapping π stacks persists. Using the TD-DFT method, some of us demonstrated H-aggregate-like effects in conjugated polymer materials^{73,74} and discovered that much more pronounced fluorescence quenching by chromophore coupling may take place when the π stack is approached by an ion.⁷⁵ Similar trends apply to phosphorescence. In fact, the first description of the chromophore coupling by Kasha was actually derived for phosphorescence from aggregates.⁷⁶ Since π stacking is a supramolecular motif observed in all structures reported here, one would reasonably expect some degree of phosphorescence quenching in all of them and a blue shift of the crystalline emission bands, compared to our predictions, computed for the molecules in solution.

For comparison, we should mention the bright emission from neat crystalline *phen*, resulting from the lack of stacking in its crystal structure. *Phen* crystallizes in the acentric C_2 space group with two crystallographically independent molecules, each forming its own herringbone-like two-dimensional layer that interleaves in the crystal.¹⁸

CONCLUSIONS

The current study enlarges the landscape of mononuclear Cu(II)–*phen* sulfates by three new members with compositions $[\text{Cu}(\text{phen})_2(\text{SO}_4)]\text{CH}_3\text{OH}$ (1), $[\text{Cu}(\text{phen})_2(\text{SO}_4)]\text{H}_2\text{O}_2\text{(DMF)}$ (2), and $[\text{Cu}(\text{phen})_2\text{H}_2\text{O}](\text{SO}_4)\text{H}_2\text{O}_4$ (3) that reveal the possibilities for accumulation of both protic and aprotic solvents in the crystal lattices. The reported examples also demonstrate the easy solvent/anion exchange that is justified by the separation of different complexes from approximately the same synthetic conditions. Crystal packing in 1–3 reveals the robust supramolecular patterns governed by the stacking interactions between the planar extended *phen* fragments being kept in all three solids regardless of the interplay of other noncovalent interactions, including rather strong hydrogen bonds. Both the *phen* ligand and complex 3 produce dual-emission spectra. Complex 3 exhibits pronounced quenching of the major emission band centered at 470 nm. The TDA-DFT calculations allow us to identify this dual emission as phosphorescence from $n-\pi$ and $\pi-\pi^*$ ligand-centered triplet

excited states. Quenching of this emission in complex 3 is explained by nonradiative decay to the low-lying triplet H-aggregate-like π -stacking and metal-centered d–d states. This property can be useful in future sensing and other technological applications of the reported complexes and their analogues.

ASSOCIATED CONTENT

Supporting Information

Synthetic procedures, selected bond distances, and full crystallographic data in CIF format for 1–3. This material is available free of charge via the Internet at <http://pubs.acs.org>. Crystallographic data for new structures reported herein were deposited with the Cambridge Crystallographic Data Centre and allocated the deposition numbers CCDC 1018815–1018817. These data can be obtained free of charge from the Cambridge Crystallographic Data Centre via www.ccdc.cam.ac.uk/data_request/cif.

AUTHOR INFORMATION

Corresponding Authors

*Fax: 373 22 725887. E-mail: fonari.xray@phys.asm.md.

*Phone: 407-374-3783. E-mail: amasunov@ucf.edu.

Notes

The authors declare no competing financial interest.

ACKNOWLEDGMENTS

This work was supported by the Russian Science Foundation, contract no. 14-43-00052. A.E.M. acknowledges the use of computational resources at The Stokes Advanced Research Computing Center, University of Central Florida (UCF), and the National Energy Research Scientific Computing Center.

REFERENCES

- (1) Kato, M.; Muto, Y. Factors Affecting the Magnetic Properties of Dimeric Copper (II) Complexes. *Coord. Chem. Rev.* **1988**, *92*, 45–83.
- (2) Santini, C.; Pellei, M.; Gandin, V.; Porchia, M.; Tisato, F.; Marzano, C. Advances in Copper Complexes as Anticancer Agents. *Chem. Rev.* **2014**, *114*, 815–862.
- (3) Halasyamani, P.; Heier, K. R.; Willis, M. J.; Stern, C. L.; Poppelman, K. R. Syntheses and Structures of Two New Cu/Nb/Pyrazine Complexes: Three Dimensional $\text{CuNb}(\text{pyz})_2\text{OF}_5$ (pyz) $-(\text{H}_2\text{O})$ and Two Dimensional $[\text{Cu}(\text{pyz})_{2.5}]^+[\text{NbF}_6]^-$ (pyz). *Z. Anorg. Allg. Chem.* **1996**, *622*, 479–485.
- (4) Darriet, J.; Haddad, J. S.; Duesler, E. N.; Hendrickson, D. N. Crystal Structure and Magnetic Properties of Bis(pyrazine)copper(II) Perchlorate, $\text{Cu}(\text{pyz})_2(\text{ClO}_4)_2$, a Two-dimensional Heisenberg Antiferromagnet. *Inorg. Chem.* **1979**, *18*, 2679–2682.
- (5) Otieno, S. J.; Rettig, R. C.; Thompson, J. Trotter, Synthesis and Structural and Magnetic Studies of Diazine-bridged Complexes of Copper(II) Cyanate. Crystal Structure of Poly[bis(cyanato-N)bis(μ -methylpyrazine)copper(II)]. *Inorg. Chem.* **1993**, *32*, 4384–4390.
- (6) Kawata, S.; Breeze, S. R.; Wang, S.; Greedan, E.; Raju, N. P. Structural Interconversion Facilitated by a Bifunctional Ligand: a Covalently Linked 2D Cu^{II} Sheet $[\text{Cu}(3\text{-pyOH})_2(\text{O}_2\text{CCF}_3)_2]_n$ and a Hydrogen-bond Linked 2D Cu^{II} Sheet $[\text{Cu}(3\text{-pyOH})_2(\text{O}_2\text{CCF}_3)_2(\text{thf})_2]_n$. *Chem. Commun.* **1997**, 717–718.
- (7) Lu, J. Y. Crystal Engineering of Cu-containing Metal–Organic Coordination Polymers Under Hydrothermal Conditions. *Coord. Chem. Rev.* **2003**, *246*, 327–347.
- (8) Cingolan, A.; Galli, S.; Masciocchi, N.; Pandolfo, L.; Pettinari, C.; Sironi, A. Sorption–Desorption Behavior of Bispyrazolato–Copper(II) 1D Coordination Polymers. *J. Am. Chem. Soc.* **2005**, *127*, 6144–6145.
- (9) Roesky, H. W.; Andruh, M. The Interplay of Coordinative, Hydrogen Bonding and $\pi-\pi$ Stacking Interactions in Sustaining

- Supramolecular Solid-State Architectures: A Study Case of Bis(4-pyridyl)- and Bis(4-pyridyl-N-oxide) Tectons. *Coord. Chem. Rev.* **2003**, *236*, 91–119.
- (10) Madalan, A. M.; Kravtsov, V. Ch.; Pajic, D.; Zadro, K.; Simonov, Yu. A.; Stanica, N.; Ouahab, L.; Lipkowski, J.; Andruh, M. Chemistry at the Apical Position of Square-Pyramidal Copper(II) Complexes: Synthesis, Crystal Structures, and Magnetic Properties of Mononuclear Cu(II), and Heteronuclear Cu(II)–Hg(II) and Cu(II)–Co(II) Complexes Containing [Cu(AA)(BB)]⁺ Moieties (AA = Acetylacetate, Salicylaldehyde; BB = 1,10-Phenanthroline, Me₂bipy = 4,4'-Dimethyl-2,2'-bipyridine). *Inorg. Chim. Acta* **2004**, *357*, 4151–4164.
- (11) Madalan, A. M.; Kravtsov, V. Ch.; Simonov, Yu. A.; Voronkova, V.; Korobchenko, L.; Avarvari, N.; Andruh, M. A. Unique Diamondoid Network Resulting from the Convolution of π–π Stacking and Lipophilic Interactions. *Cryst. Growth Des.* **2005**, *5*, 45–47.
- (12) McCann, M.; McGinley, J.; Ni, K.; O'Connor, M.; Kavanagh, K.; McKee, V.; Colleran, J.; Devereux, M.; Gathergood, N.; Barron, N.; et al. A New Phenanthroline–Oxazine Ligand: Synthesis, Coordination Chemistry and Atypical DNA Binding Interaction. *Chem. Commun.* **2013**, *49*, 2341–2343.
- (13) Garzon-Rodriguez, W.; Yatsimirsky, A. K.; Glabe, C. G. Binding of Zn(II), Cu(II), and Fe(II) ions to Alzheimer's Aβ Peptide Studied by Fluorescence. *Bioorg. Med. Chem. Lett.* **1999**, *9*, 2243–2248.
- (14) Syme, C. D.; Nadal, R. C.; Rigby, S. E. J.; Viles, J. H. Copper Binding to the Amyloid-β (Aβ) Peptide Associated with Alzheimer's Disease. Folding, Coordination Geometry, pH Dependence, Stoichiometry, and Affinity of Aβ(1–28): Insight from a Range of Complementary Spectroscopic Techniques. *J. Biol. Chem.* **2004**, *279*, 18169–18177.
- (15) Stöckel, J.; Safar, J.; Wallace, A. C.; Cohen, F. E.; Prusiner, S. B. Prion Protein Selectively Binds Copper(II) Ions. *Biochemistry* **1998**, *37*, 7185–7193.
- (16) Sheldrick, G. M. A Short History of SHELLX. *Acta Crystallogr.* **2008**, *A64*, 112–122.
- (17) Macrae, C. F.; Edgington, P. R.; McCabe, P.; Pidcock, E.; Shields, G. P.; Taylor, R.; Towler, M.; van de Streek, J. Mercury: Visualization and Analysis of Crystal Structures. *J. Appl. Crystallogr.* **2006**, *39*, 453–457.
- (18) Nishigaki, S.; Yoshioka, H.; Nakatsu, K. The Crystal and Molecular Structure of o-Phenanthroline. *Acta Crystallogr.* **1978**, *B34*, 875–879.
- (19) Frisch, M. J.; Trucks, G. W.; Schlegel, H. B.; Scuseria, G. E.; Robb, M. A.; Cheeseman, J. R.; Scalmani, G.; Barone, V.; Mennucci, B.; Petersson, G. A.; et al. Gaussian 09, Revision D.01; Gaussian, Inc.: Wallingford, CT, 2009.
- (20) Dunning, T. H., Jr.; Hay, P. J. In *Modern Theoretical Chemistry*. Schaefer, H. F., III, Ed.; Plenum: New York, 1977; Vol. 3, pp 1–21.
- (21) Mikhailov, I. A.; Bondar, M. V.; Belfield, K. D.; Masunov, A. E. Electronic Properties of a New Two-Photon Absorbing Fluorene Derivative: The Role of Hartree-Fock Exchange in the Density Functional Theory Design of Improved Nonlinear Chromophores. *J. Phys. Chem. C* **2009**, *113*, 20719–20724.
- (22) Zhao, Y.; Schultz, N. E.; Truhlar, D. G. Design of Density Functionals by Combining the Method of Constraint Satisfaction with Parametrization for Thermochemistry, Thermochemical Kinetics, and Noncovalent Interactions. *J. Chem. Theory Comput.* **2006**, *2*, 364–382.
- (23) Liu, J. H.; Mikhaylov, I. A.; Zou, J. H.; Osaka, I.; Masunov, A. E.; McCullough, R. D.; Zhai, L. Insight into How Molecular Structures of Thiophene-based Conjugated Polymers Affect Crystallization Behaviors. *Polymer* **2011**, *52*, 2302–2309.
- (24) Mikhailov, I. A.; Belfield, K. D.; Masunov, A. E. DFT-Based Methods in the Design of Two-Photon Operated Molecular Switches. *J. Phys. Chem. A* **2009**, *113*, 7080–7089.
- (25) De Boni, L.; Toro, C.; Masunov, A. E.; Hernandez, F. E. Untangling the Excited States of DR1 in Solution: An Experimental and Theoretical Study. *J. Phys. Chem. A* **2008**, *112*, 3886–3890.
- (26) Toro, C.; Thibert, A.; De Boni, L.; Masunov, A. E.; Hernandez, F. E. Fluorescence Emission of Disperse Red 1 in Solution at Room Temperature. *J. Phys. Chem. B* **2008**, *112*, 929–937.
- (27) Nayyar, I. H.; Masunov, A. E.; Tretiak, S. Comparison of TD-DFT Methods for the Calculation of Two-Photon Absorption Spectra of Oligophenylvinyles. *J. Phys. Chem. C* **2013**, *117*, 18170–18189.
- (28) Masunov, A. E.; Mikhailov, I. A. Theory and Computations of Two-Photon Absorbing Photochromic Chromophores. *Eur. J. Chem.* **2010**, *1*, 142–161.
- (29) Casida, M. E.; Huix-Rotllant, M. Progress in Time-Dependent Density-Functional Theory. *Annu. Rev. Phys. Chem.* **2012**, *63*, 287–323.
- (30) Hirata, S.; Head-Gordon, M. Time-Dependent Density Functional Theory within the Tamm–Dancoff Approximation. *Chem. Phys. Lett.* **1999**, *314*, 291–299.
- (31) Marenich, A. V.; Cramer, C. J.; Truhlar, D. G. Universal Solvation Model Based on Solute Electron Density and on a Continuum Model of the Solvent Defined by the Bulk Dielectric Constant and Atomic Surface Tensions. *J. Phys. Chem. B* **2009**, *113*, 6378–6396.
- (32) Healy, P. C.; Patrick, J. M.; White, A. H. Crystal structure of Diaqua(1,10-phenanthroline)copper(II) Sulfate. *Aust. J. Chem.* **1984**, *37*, 1111–1115.
- (33) Gong, Y.-N.; Liu, C.-B.; Tang, X.-H.; Zhang, A.-Q. Formation of a 1-D Metal–Water Chain and a 2-D Water–Sulfate Layer Containing Cyclic Water Octamers in a 3-D Supramolecular Network. *J. Coord. Chem.* **2011**, *46*, 2761–2769.
- (34) Meundaeng, N.; Prior, T. J.; Rujiwatrat, A. Bis(1,10-phenanthroline-²N,N')(sulfato-O)copper(II) Ethanol Monosolvate. *Acta Crystallogr.* **2013**, *E69*, m568–m569.
- (35) Zhong, K.-L. Bis(1,10-phenanthroline-²N,N')(sulfato-O)copper(II) Ethane-1,2-diol Monosolvate. *Acta Crystallogr.* **2011**, *E67*, m1215–m1216.
- (36) Zhong, K.-L. Bis(1,10-phenanthroline-²N,N')(sulfato-O)copper(II) Propane-1,3-diol Monosolvate. *Acta Crystallogr.* **2012**, *E68*, m1555.
- (37) Zhong, K.-L. Crystal Structure of Bis(1,10-phenanthroline-κ²N,N')(sulfato-κ²O,O')-copper(II)–Propane-1,2-diol (1:1), Cu(C₁₂H₈N₂)₂(SO₄)C₃H₈O₂. *Z. Kristallogr.–New Cryst. Struct.* **2011**, *226*, 286–288.
- (38) Zhong, K.-L.; Cao, G.-Q. Bis(1,10-phenanthroline-²N,N')(sulfato-O)copper(II) Butane-2,3-diol Monosolvate. *Acta Crystallogr.* **2013**, *E69*, m40–m41.
- (39) Youngme, S.; Wannarit, N.; Pakawatchai, C.; Chaichit, N.; Somsook, E.; Turpeinen, U.; Mutikainen, I. Structural Diversities and Spectroscopic Properties of Bis and Tris(1,10-phenanthroline) Copper(II) Complexes. *Polyhedron* **2007**, *26*, 1459–1468.
- (40) Addison, A. W.; Rao, T. N.; Reedijk, J.; van Rijn, J.; Verschoor, G. C. Synthesis, Structure, and Spectroscopic Properties of Copper(II) Compounds Containing Nitrogen-Sulphur Donor Ligands; the Crystal and Molecular Structure of Aqua[1,7-bis(N-methylbenzimidazol-2'-yl)-2,6-dithiaheptane] Copper(II) Perchlorate. *J. Chem. Soc., Dalton Trans.* **1984**, 1349–1356.
- (41) Reger, D. L.; Pascui, A. E.; Smith, M. D.; Jezierska, J.; Ozarowski, A. Dinuclear Complexes Containing Linear M–F–M [M = Mn(II), Fe(II), Co(II), Ni(II), Cu(II), Zn(II), Cd(II)] Bridges: Trends in Structures, Antiferromagnetic Superexchange Interactions, and Spectroscopic Properties. *Inorg. Chem.* **2012**, *51*, 11820–11836.
- (42) Pasquarello, A.; Petri, I.; Salmon, P. S.; Parisel, O.; Car, R.; Tóth, É.; Powell, D. H.; Fischer, H. E.; Helm, L.; Merbach, A. E. First Solvation Shell of the Cu(II) Aqua Ion: Evidence for Fivefold Coordination. *Science* **2001**, *291*, 856–859.
- (43) Janiak, C. A Critical Account on π–π Stacking in Metal Complexes with Aromatic Nitrogen-Containing Ligands. *J. Chem. Soc., Dalton Trans.* **2000**, 3885–3896.
- (44) Janjić, G. V.; Petrović, P. V.; Ninković, D. B.; Zarić, S. D. Geometries of Stacking Interactions between Phenanthroline Ligands in Crystal Structures of Square-Planar Metal Complexes. *J. Mol. Model.* **2011**, *17*, 2083–2092.
- (45) Petrović, P. V.; Janjić, G. V.; Zarić, S. D. Stacking Interactions between Square-Planar Metal Complexes with 2,2'-Bipyridine Ligands.

- Analysis of Crystal Structures and Quantum Chemical Calculations. *Cryst. Growth Des.* **2014**, *14*, 3880–3889.
- (46) Horn, C.; Ali, B.; Dance, I.; Scudder, M.; Craig, D. Crystal Supramolecularity: Extended Aryl Embraces in Dimorphs of $[Cu(1,10-phen)_2I]I_3$. *CrystEngComm* **2000**, *2*, 6–15.
- (47) Dance, I.; Scudder, M. Molecules Embracing in Crystals. *CrystEngComm* **2009**, *11*, 2233–2247.
- (48) Etter, M. C. Encoding and Decoding Hydrogen-Bond Patterns of Organic Compounds. *Acc. Chem. Res.* **1990**, *23*, 120–126.
- (49) Liu, Z.-C.; Yang, Z.-Y.; Li, T.-R.; Wang, B.-D.; Li, Y.; Qin, D.-D.; Wang, M.-F.; Yan, M.-H. An Effective Cu(II) Quenching Fluorescence Sensor in Aqueous Solution and 1D Chain Coordination Polymer Framework. *Dalton Trans.* **2011**, *40*, 9370–9373.
- (50) Esteves da Silva, J. C. G.; Machado, A. A. S. C.; Oliveira, C. J. S.; Pinto, M. S. S. D. S. Fluorescence quenching of anthropogenic fulvic acids by Cu(II), Fe(III) and UO_2^{2+} . *Talanta* **1998**, *45*, 1155–1165.
- (51) Royzen, M.; Dai, Z.; Canary, J. W. Ratiometric Displacement Approach to Cu(II) Sensing by Fluorescence. *J. Am. Chem. Soc.* **2005**, *127*, 1612–1613.
- (52) de Silva, A. P.; Gunaratne, H. Q. N.; Gunnlaugsson, T.; Huxley, A. J. M.; McCoy, C. P.; Rademacher, J. T.; Rice, T. E. Signaling Recognition Events with Fluorescent Sensors and Switches. *Chem. Rev.* **1997**, *97*, 1515–1566.
- (53) Accorsi, G.; Listorti, A.; Yoosaf, K.; Armaroli, N. 1,10-Phenanthrolines: Versatile Building Blocks for Luminescent Molecules, Materials and Metal Complexes. *Chem. Soc. Rev.* **2009**, *38*, 1690–1700.
- (54) Armaroli, N.; De Cola, L.; Balzani, V.; Sauvage, J.-P.; Dietrich-Buchecker, C. O.; Kern, J.-M. Absorption and Luminescence Properties of 1,10-Phenanthroline, 2,9-Diphenyl-1,10-Phenanthroline, 2,9-Dianisyl-1,10-Phenanthroline and Their Protonated Forms in Dichloromethane Solution. *J. Chem. Soc., Faraday Trans.* **1992**, *88*, 553–556.
- (55) Bandyopadhyay, B. N.; Harriman, A. Photoreduction of 1,10-Phenanthroline. *J. Chem. Soc., Faraday Trans. 1* **1977**, *73*, 663–674.
- (56) Barbieri, A.; Accorsi, G.; Armaroli, N. Luminescent Complexes Beyond the Platinum Group: the d¹⁰ Avenue. *Chem. Commun.* **2008**, 2185–2193.
- (57) Armaroli, N.; De Cola, L.; Balzani, V.; Sauvage, J.-P.; Dietrich-Buchecker, C. O.; Kern, J.-M.; Bailal, A. Absorption and Emission Properties of a 2-Catenand, its Protonated Forms, and its Complexes with Li⁺, Cu⁺, Ag⁺, Co²⁺, Ni²⁺, Zn²⁺, Pd²⁺ and Cd²⁺: Tuning of the Luminescence Over the Whole Visible Spectral Region. *J. Chem. Soc., Dalton Trans.* **1993**, 3241–3247.
- (58) Armaroli, N.; Accorsi, G.; Cardinali, F.; Listorti, A. Photochemistry and Photophysics of Coordination Compounds: Copper. *Top. Curr. Chem.* **2007**, *280*, 69–115.
- (59) Mistri, S.; Garcia-Granda, S.; Zangrando, E.; Manna, S. C. Fluorescent Bis-Chelated-1,10-Phenanthroline-Azido-Copper(II) Complex for Selective Sensing of Aniline. *Polyhedron* **2013**, *50*, 333–338.
- (60) Mistri, S.; Zangrando, E.; Manna, S. C. Tetracarboxylato-bridged Copper(II) Complexes with Ancillary N-Chelating Ligands: Syntheses, Crystal Structures and Effect of Aromatic Compounds on the Fluorescence Property. *Polyhedron* **2013**, *49*, 252–258.
- (61) Cardenas-Jiron, G. I.; Masunov, A.; Dannenberg, J. J. Molecular Orbital Study of Crystalline p-Benzquinone. *J. Phys. Chem. A* **1999**, *103*, 7042–7046.
- (62) Masunov, A. E.; Zorkii, P. M. Geometric Characteristics of Halogen-Halogen Intermolecular Contacts in Organic Crystals. *Zh. Fiz. Khim.* **1992**, *66*, 60–69.
- (63) Passier, R.; Ritchie, J. P.; Toro, C.; Diaz, C.; Masunov, A. E.; Belfield, K. D.; Hernandez, F. E. Thermally Controlled Preferential Molecular Aggregation State in a Thiocarbocyanine Dye. *J. Chem. Phys.* **2010**, *133*, 13450 (1–7).
- (64) Gadzhiev, O. B.; Ignatov, S. K.; Razuvayev, A. G.; Masunov, A. E. Quantum Chemical Study of Trimolecular Reaction Mechanism between Nitric Oxide and Oxygen in the Gas Phase. *J. Phys. Chem. A* **2009**, *113*, 9092–9101.
- (65) Patel, P. D.; Masunov, A. E. Theoretical Study of Photochromic Compounds: Part 3. Prediction of Thermal Stability. *J. Phys. Chem. C* **2011**, *115*, 10292–10297.
- (66) Kuchma, M. H.; Komanski, C. B.; Colon, J.; Teblum, A.; Masunov, A. E.; Alvarado, B.; Babu, S.; Seal, S.; Summy, J.; Baker, C. H. Phosphate Ester Hydrolysis of Biologically Relevant Molecules by Cerium Oxide Nanoparticles. *Nanomedicine: NBM* **2010**, *6*, 738–744.
- (67) Belfield, K. D.; Bondar, M. V.; Hernandez, F. E.; Masunov, A. E.; Mikhailov, I. A.; Morales, A. R.; Przhonska, O. V.; Yao, S. Two-Photon Absorption Properties of New Fluorene-Based Singlet Oxygen Photosensitizers. *J. Phys. Chem. C* **2009**, *113*, 4706–4711.
- (68) Belfield, K. D.; Bondar, M. V.; Frazer, A.; Morales, A. R.; Kachkovsky, O. D.; Mikhailov, I. A.; Masunov, A. E.; Przhonska, O. V. Fluorene-Based Metal-Ion Sensing Probe with High Sensitivity to Zn²⁺ and Efficient Two-Photon Absorption. *J. Phys. Chem. B* **2010**, *114*, 9313–9321.
- (69) Webster, S.; Peceli, D.; Hu, H.; Padilha, L. A.; Przhonska, O. V.; Masunov, A. E.; Gerasov, A. O.; Kachkovski, A. D.; Slominsky, Y. L.; Tolmachev, A. I.; et al. Near-Unity Quantum Yields for Intersystem Crossing and Singlet Oxygen Generation in Polymethine-like Molecules: Design and Experimental Realization. *J. Phys. Chem. Lett.* **2010**, *1*, 2354–2360.
- (70) Ganin, E. V.; Masunov, A. E.; Siminel, A. V.; Fonari, M. S. Preparation, Characterization, and Electronic Structure of Asymmetric Isonaphthalimide: Mechanism of Dual Fluorescence in Solid State. *J. Phys. Chem. C* **2013**, *117*, 18154–18162.
- (71) Croitor, L.; Coropceanu, E. B.; Siminel, A. V.; Masunov, A. E.; Fonari, M. S. From Discrete Molecules to One-dimensional Coordination Polymers Containing Mn(II), Zn(II) or Cd(II) Pyridine-2-aldoxime Building Unit. *Polyhedron* **2013**, *60*, 140–150.
- (72) Spano, F. C. Excitons in Conjugated Oligomer Aggregates, Films, and Crystals. *Annu. Rev. Phys. Chem.* **2006**, *57*, 217–243.
- (73) Crotty, A. M.; Gizzi, A. N.; Rivera-Jacquez, H. J.; Masunov, A. E.; Hu, Z.; Geldmeier, J. A.; Gesquiere, A. J. Molecular Packing in Organic Solar Cell Materials: Insights from the Emission Line Shapes of P3HT/PCBM Polymer Blend Nanoparticles. *J. Phys. Chem. C* **2014**, *118*, 19975–19984.
- (74) Liu, J. H.; Mikhailov, I. A.; Zou, J. H.; Osaka, I.; Masunov, A. E.; McCullough, R. D.; Zhai, L. Insight into How Molecular Structures of Thiophene-based Conjugated Polymers Affect Crystallization Behaviors. *Polymer* **2011**, *52*, 2302–2309.
- (75) Masunov, A.; Tretiak, S.; Hong, J. W.; Liu, B.; Bazan, G. C. Theoretical Study of the Effects of Solvent Environment on Photophysical Properties and Electronic Structure of Paracyclophane Chromophores. *J. Chem. Phys.* **2005**, *122*, No. 224505.
- (76) McRae, E. G.; Kasha, M. Enhancement of Phosphorescence Ability upon Aggregation of Dye Molecules. *J. Chem. Phys.* **1958**, *28*, 721–722.

■ NOTE ADDED AFTER ASAP PUBLICATION

This paper was published to the Web on December 11, 2014, with errors in Figure 8 and the Acknowledgments. These were corrected in the version published to the Web on December 15, 2014.